Journal of Structural Geology 31 (2009) 737–748

Contents lists available at ScienceDirect

Journal of Structural Geology

journal homepage: www.elsevier.com/locate/jsg

NE–SW-trending Hepu–Hetai dextral shear zone in southern China: Penetration of the Yunkai Promontory of South China into Indochina

Kai-Jun Zhang [a,b,*], Jian-Xin Cai [a,c]

[a] Guangzhou Institute of Geochemistry, Chinese Academy of Sciences, Guangzhou 510640, China
[b] Department of Earth Sciences, Nanjing University, Nanjing 210093, China
[c] Graduate School, Chinese Academy of Sciences, Beijing 100008, China

ARTICLE INFO

Article history:
Received 8 August 2008
Received in revised form
25 April 2009
Accepted 28 April 2009
Available online 7 May 2009

Keywords:
South China
Indochina
Ductile shear zone
Plate tectonics
Irregular continental margin
Mesozoic

ABSTRACT

The NE–SW-trending Hepu–Hetai shear zone extends for about 480 km along the boundary between Guangdong and Guangxi provinces in the southern part of South China. Field mapping and kinematic analyses indicate that the zone is characterized by dextral ductile strike-slip deformation, with an estimated displacement along the fault zone in excess of 500 km. Studies of synkinematic phengite and gas–liquid inclusions in quartz within mylonite suggest that the ductile shear deformation occurred under medium temperature/pressure conditions of the greenschist facies, and $^{40}Ar/^{39}Ar$ analyses of muscovite yield ages of 213–195 Ma. Based on these data and Late Paleozoic–Mesozoic paleogeographic data for southern China, we propose that the Hepu–Hetai shear zone originated via the penetration of the Yunkai Promontory of South China into Indochina during the Triassic.

1. Introduction

The Mesozoic tectonic history of SE Asia was dominated by the amalgamation of several continental blocks (including South China, Indochina, Simao, Sibumasu and West Burma) with the Asian continent (Hutchison, 1993; Metcalfe, 2002; Lepvrier et al., 2004) (Fig. 1A). These events were accompanied by closure of the Paleotethys (Hutchison, 1993; Metcalfe, 2002; Zhang et al., 2002), which resulted in a series of deformation events within the accreted blocks and at their mutual boundaries. Such deformation structures have long been valued by geologists in terms of deciphering the tectonic processes involved in the accretion of terranes.

One such example of deformation structures is the Truong belt in north–central Vietnam, which contains several sub-parallel NW–SE to E–W-trending dextral fault zones of Early–Middle Triassic age (Findlay and Phan, 1997; Lacassin et al., 1998; Lepvrier et al., 2004). Coeval deformation is found along the southern margin of South China, which contains several fault zones that vary in trend from nearly E–W to NE–SW; however, the kinematics and timing of these fault zones remain a matter of debate (Hsü et al., 1990; Liang and Li, 2005; Wang et al., 2007).

The Hepu–Hetai shear zone (Fig. 1B), which represents the easternmost portion of the NE–SW-trending shear zones, is a key feature of the geology of the southern margin of South China. Previous studies have proposed conflicting accounts of its kinematics, geochronology, and tectonic setting (Ling et al., 1992; Zhang and Yu, 1992; Wang et al., 1994; Peng et al., 1995; Liang and Li, 2005; Wang et al., 2007). The shear zone is generally viewed as the boundary fault between the Yangtze and Cathysia blocks within South China, given the sporadic occurrence of serpentinized mafic and ultramafic fragments along the zone (e.g., Qin et al., 2005; Peng et al., 2006a). Here, we investigate the nature of ductile dextral strike-slip deformation along the shear zone and propose a new tectonic model for collision between South China and Indochina.

2. Regional geology

2.1. Yunkai Promontory

On the east of the Hepu–Hetai shear zone is the Yunkai Promontory, which includes the Yunkai and northern Hainan regions (Fig. 1B). The siliciclastic-dominated Sinian to Ordovician strata in

* Corresponding author. Guangzhou Institute of Geochemistry, Chinese Academy of Sciences, Guangzhou 510640, China. Fax: +86 20 8529 0231.
E-mail addresses: kaijun@gig.ac.cn, kjzhang@nju.edu.cn (K.-J. Zhang).

0191-8141/$ – see front matter © 2009 Elsevier Ltd. All rights reserved.
doi:10.1016/j.jsg.2009.04.012

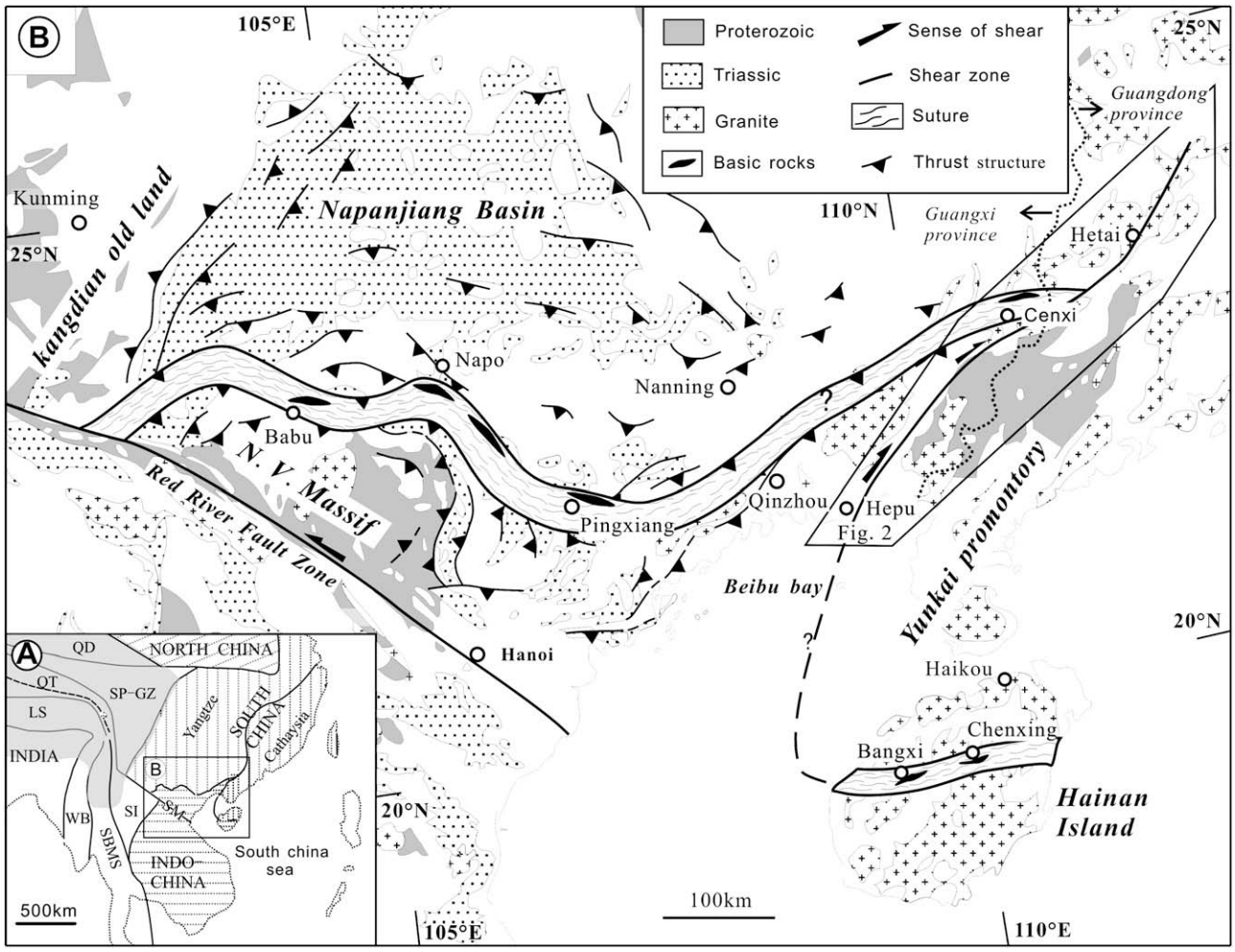

Fig. 1. (A) Sketch tectonic map of eastern Asia, revised after Zhang et al. (2002). Abbreviations: LS, Lhasa; QD, Qaidam; QT, Qiangtang; SBMS, Sibumasu; SI, Simao; SM, Song Ma; SP–GZ, Songpan–Ganzi; WB, West Burma. (B) Sketch geologic map of the southern margin of South China, showing the main tectonic units in southern China and Vietnam: The dash line outlines the likely plate boundary between South China and Indochina. The Hepu–Hetai shear zone is shown by the thick line. Revised after CAGS (1975) and Zhang et al. (2002).

these regions differ from the carbonate-dominated strata in southern Hainan and northern Vietnam (GBGMR, 1985; GBGMR, 1988). In the Yunkai region, the promontory consists of a widespread metamorphic complex that is generally believed to represent the Precambrian basement (2702–1616 Ma) of the Cathysian block (Zhang et al., 1998; Huang et al., 2001; Qin et al., 2006). These metamorphic rocks were locally remobilized during a Caledonian thermotectonic event that yielded 467–394 Ma anatectic granites (Wang et al., 1999; Peng et al., 2006b). Granitoids of 269–201 Ma in age (GBGMR, 1988; Ye, 1989; Zhang and Yu, 1992) also occur in the region, mainly along the shear zone. Upper Paleozoic to Mesozoic siliciclastic rocks of coastal facies are generally absent from the promontory, except for at its margin.

2.2. Nanpanjiang Basin

The Nanpanjiang Basin, located east of the Kangdian old land (Fig. 1B), is largely covered by Lower–Middle Triassic turbidites, which are in turn locally unconformably overlain by rare Upper Triassic terrestrial clastic rocks. Lower Paleozoic strata are dominated by siliciclastic rocks (GBGMR, 1985; YNGMR, 1990), and the Upper Paleozoic series, up to 1500–3000 m thick, occurs dominantly as isolated platform deposits or deep-water basin deposits (GBGMR, 1985)—this pattern continued until the Middle Triassic (Lehrmann et al., 2007; Enos et al., 1998). The platform facies is dominantly limestone, with minor basic volcanics. Surrounding this shallow-water facies is a basin succession of pelagic to hemipelagic argillaceous rocks, chert, and chert-bearing limestone, intercalated with basic to intermediate volcanics (GBGMR, 1985). Throughout most of the basin, Upper Paleozoic and Lower–Middle Triassic rocks have been intensively deformed, resulting in well-developed fold and thrust structures with variable trend (Fig. 1B). In the eastern part of the basin, however, these Indosinian structures are completely overprinted by NE–SW-striking deformation structures related to Late Mesozoic subduction of the Pacific Plate (Liang and Li, 2005; Zhou et al., 2006; Wang et al., 2007).

2.3. Plate suture

The occurrence of sporadic ophiolitic fragments along the China–Vietnam border suggests the presence of a tectonic suture (Wu et al., 1999) (Fig. 1B). Mid-ocean ridge basalt (MORB)-type mafic and ultramafic rocks with an age of 328 Ma have been reported from Babu (Zhong et al., 1998; Wu et al., 2001). This suture can be traced eastward along the China–Vietnam border through

Napo to Pingxiang, where oceanic island or island-arc tholeiites of the Permian to Early Triassic are exposed in nappe sheets transported from the south (Wu et al., 2000, 2002). Therefore, this part of the suture represents its northern limit. To the northeast, at Cenxi, on the border between Guangdong and Guangxi provinces of southern China, basic rock associations have been identified in Silurian to Carboniferous shales, carbonates, and cherts (Zhang et al., 1995) (Fig. 1B). These rocks, which include spilites, keratophyres, pillow basalts, and volcanic breccias, are of island-arc affinity and are Late Permian in age (^{40}Ar–^{39}Ar age of ~255 Ma) (Zhang et al., 2003).

This suture also extends into the central part of Hainan Island in southernmost China, as indicated by the occurrence of metamorphosed Upper Paleozoic mafic rocks in Bangxi and Chenxing (Li et al., 2000a,b, 2002) (Fig. 1B). These rocks have been dated at 333 Ma (Sm–Nd isochron method) and have typical MORB characteristics: they are depleted in Th and light rare earth elements, and enriched in Nb and Ta, with high positive $\varepsilon_{Nd\,(t)}$ values (~+7).

Clearly, this suture (the Dian–Qiong suture) separates the Chinese mainland (with a Cathysian affinity) to the north and southern Hainan Island and northern Vietnam (with an Indochina affinity; e.g., Hsü et al., 1990) to the south (Figs. 1A,B), thereby representing the main tectonic divide between the Cathysian and Indochina blocks. The ophiolitic fragments that occur along the suture zone are relics of the oceanic environment present between these two continents during the Late Paleozoic to Triassic (e.g., Zhong et al., 1998; Li et al., 2000a,b, 2002; Wu et al., 2001; Zhang et al., 2003).

3. Geometry and kinematics of the Hepu–Hetai shear zone

The Hepu–Hetai shear zone extends for ~480 km with a NE–SW trend, from north of Hetai to Hepu in the south near Beibu Bay (Fig. 2). Along this zone, pre-Mesozoic formations and granites are strongly deformed and metamorphosed to produce sub-parallel metamorphic bands varying in grade from greenschist to amphibolite facies (GBGMR, 1985; GBGMR, 1988). The shear zone is locally intruded by undeformed post-Triassic granites and overlain by Cretaceous to Tertiary coarse-grained terrestrial redbeds. The zone can be subdivided into three distinct segments based on its trend. Each of these segments is considered below.

3.1. Hetai–Guangning segment

The Hetai–Guangning segment (the northernmost of the three segments) trends approximately N45°E through the Guangning metamorphic complex and ends to the northeast in the Dayao Shan uplift (Fig. 2). Farther north, in the Xinzhou area, the shear zone is replaced by nappe structures consisting of pre-Cambrian metamorphic rocks thrust over a Devonian–Carboniferous shelf series (Peng et al., 1990).

The Guangning complex comprises granites, migmatites, and irregularly distributed metamorphic rocks. Ductile shear belts occur between the granites and metamorphic rocks, especially within migmatites. A NE–SW-striking foliation with a subhorizontal lineation is found throughout the entire area. For example, ~13 km southeast of Guangning, this type of shear deformation overprints migmatites, yielding a distinct NE–SW-striking foliation defined by

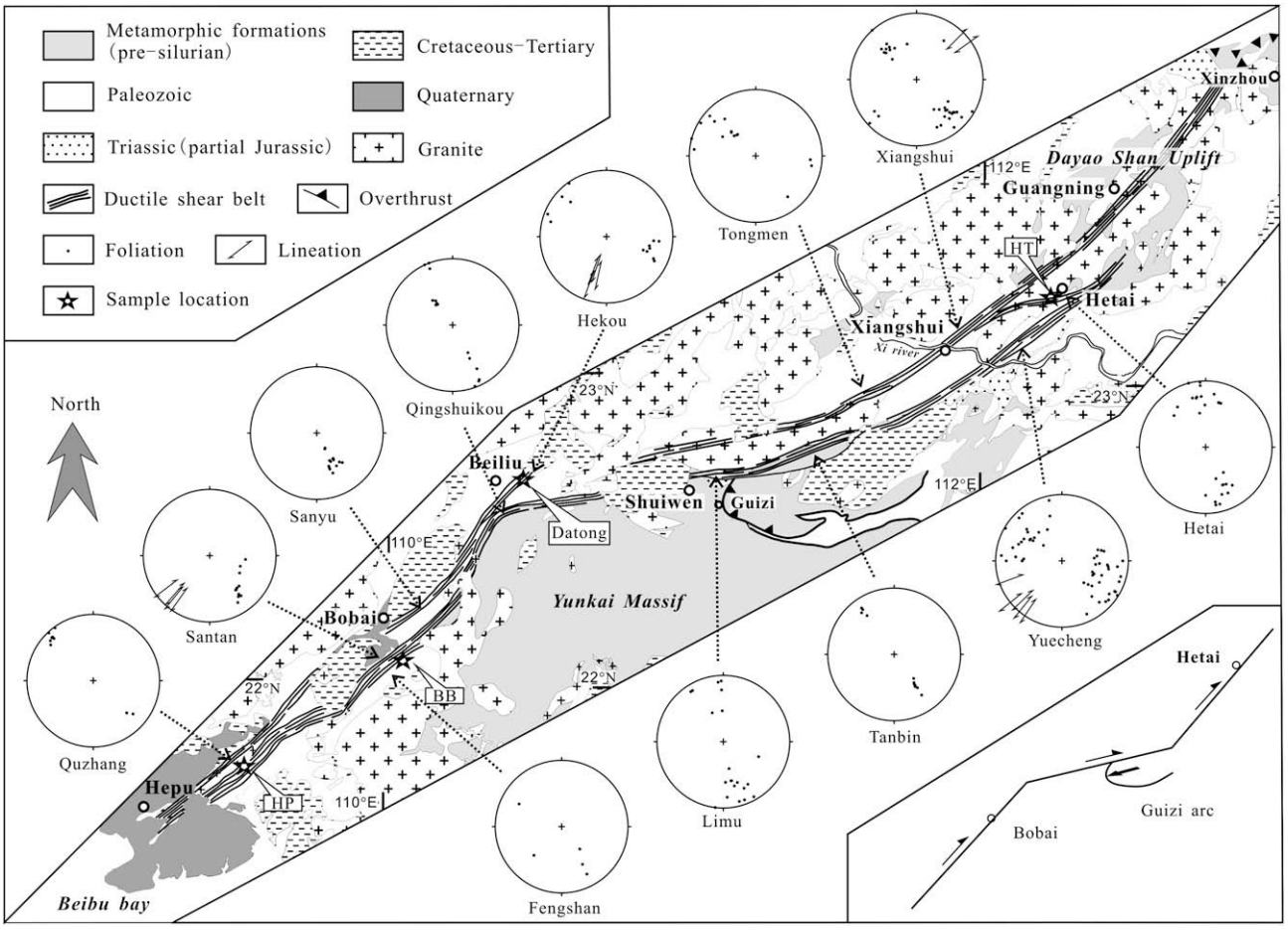

Fig. 2. Simplified geologic map of the Hepu–Hetai shear zone, revised after GXGMR (1985) and GDGMR (1988) with our own observations. The attitudes of mylonitic foliation and stretching lineation are shown by polar projection. The kinematic model of the shear zone is roughly demonstrated in the bottom-right corner.

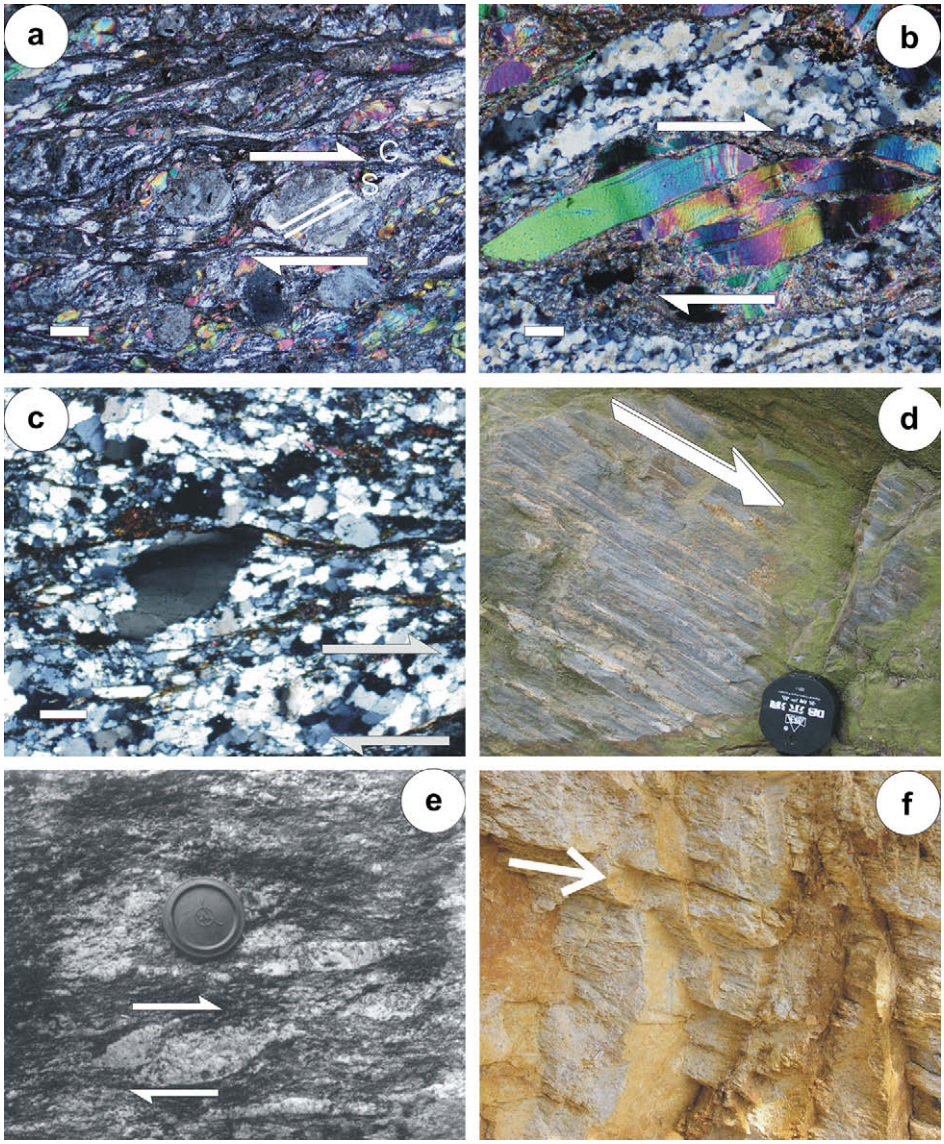

Fig. 3. Representative micrographs (a, b, c, scale bar = 1000 μm) and field pictures (d, e, f) of the Hepu–Hetai shear zone; sections are in a horizontal plane perpendicular to the mylonitic foliation and parallel to the stretching lineation. (a) Well-defined S–C fabrics in the mylonites, from Hetai. The white paired arrows indicate a dextral motion. (b) The domino structure of mica showing a dextral motion, from Hetai. (c) Re-crystallized quartzes in the mylonites and their preferred orientation, from Bobai. (d) Steeply NW-dipping foliations with a NE–SW trend, from Xiangshui (top view). White arrows indicate the attitude of the foliation. (e) Sheared quartz veins (top view), from Bobai. (f) Nearly horizontal stretching lineation with a NE–SW trend, from Bobai.

Table 1
Homogenization temperatures and corresponding trapped temperatures of the gas–liquid inclusions in quartz within the mylonites from the Hepu–Hetai shear zone.

Homogenization temperature (°C)	Trapped temperature (°C)
HP-1 (Hepu)	
238, 254, 260, 250, 248, 272, 175	404, 423, 430, 418, 416, 446, 333
BB-1 (Bobai)	
175, 168, 175, 226, 229, 212, 215, 210, 213, 221, 228, 224, 215, 236, 218	333, 325, 333, 390, 394, 374, 378, 372, 376, 385, 393, 388, 378, 402, 381
BB-2 (Bobai)	
144, 146, 142, 235, 218, 220, 217, 189	300, 302, 298, 401, 381, 384, 380, 348
HT-44 (Hetai)	
156, 147, 155, 152, 290, 310	312, 303, 311, 308, 469, 496

See Fig. 2 for the sampling locations. The inclusion trapped temperatures were estimated roughly according to the empirical plots of Potter (1977), under the different stress mostly between 1.6 and 2.1 kb estimated by quartz subgrain method (Mercier, 1977; Twiss, 1977) and considering the NaCl concentrations have little effect on the trapped temperatures.

Table 2
Analyses of the muscovites in the mylonites from the Hepu–Hetai shear zone (wt %).

SiO_2		TiO_2	Al_2O_3	FeO	MnO	MgO	CaO	Na_2O	K_2O	P_2O_5	Total
HP-1 (Hepu)											
1	49.88	0.29	30.90	4.74	0.00	1.67	0.00	0.23	9.09	0.02	96.81
2	49.64	0.57	30.10	4.33	0.03	1.34	0.00	0.16	9.73	0.01	95.91
3	48.10	0.54	31.25	4.22	0.02	1.39	0.00	0.22	10.56	0.02	96.31
4	49.88	0.36	30.43	3.93	0.02	1.26	0.00	0.11	9.51	0.00	95.51
5	49.46	0.67	31.41	4.45	0.03	1.05	0.00	0.09	9.63	0.03	96.78
BB-1 (Bobai)											
1	50.39	0.75	29.64	4.58	0.01	1.95	0.00	0.17	8.75	0.04	96.24
2	50.49	0.54	29.11	5.22	0.00	1.68	0.00	0.11	9.34	0.00	96.48
3	50.56	0.58	28.33	5.01	0.00	1.71	0.00	0.09	9.42	0.00	95.67
4	50.07	0.93	29.18	5.13	0.00	1.55	0.00	0.07	9.46	0.00	96.40
5	49.40	1.11	29.15	4.67	0.00	1.33	0.00	0.08	9.90	0.00	95.65
BB-2 (Bobai)											
1	49.80	0.19	30.30	4.50	0.04	1.37	0.00	0.11	9.82	0.02	96.13
2	49.94	0.40	31.61	2.37	0.01	1.63	0.00	0.13	9.30	0.00	95.39
3	50.05	0.27	30.13	4.26	0.00	1.14	0.00	0.11	9.91	0.00	95.86
4	48.99	0.40	29.89	4.77	0.00	1.57	0.00	0.12	9.73	0.00	95.46
5	49.65	0.20	29.09	4.84	0.03	2.01	0.00	0.14	9.17	0.02	95.13
HT-1 (Hetai)											
1	49.07	0.00	33.39	2.23	0.01	1.18	0.06	0.12	9.68	0.02	95.75
2	49.89	0.08	33.49	1.66	0.02	1.09	0.00	0.09	9.97	0.00	96.29
3	50.36	0.17	32.18	1.86	0.00	0.93	0.00	0.12	10.18	0.00	95.81
4	49.10	0.17	34.60	1.47	0.02	0.81	0.00	0.16	9.91	0.00	96.24
5	48.75	0.16	34.32	1.97	0.00	1.29	0.00	0.12	9.82	0.01	96.44
HT-44 (Hetai)											
1	48.78	0.36	33.00	2.39	0.03	1.58	0.00	0.18	9.35	0.00	95.68
2	47.81	0.23	34.95	1.94	0.01	1.12	0.00	0.27	9.56	0.07	95.89
3	47.34	0.71	36.61	1.06	0.00	0.58	0.00	0.41	9.37	0.00	96.07
4	47.70	0.50	34.48	2.36	0.00	1.30	0.00	0.27	9.76	0.02	96.36
5	47.96	0.53	33.64	2.94	0.00	1.67	0.00	0.21	9.65	0.01	96.60
Si^{4+}		Ti^{4+}	$Al^{3+}IV$	$Al^{3+}IX$	Fe^{3+}	Fe^{2+}	Mn^{2+}	Mg^{2+}	Ca^{2+}	Na^{+}	K^{+}
BB-1 (Bobai)											
1	3.308	0.037	0.692	1.601	0.130	0.107	0.001	0.191	0.000	0.021	0.732
2	3.327	0.027	0.673	1.588	0.126	0.148	0.000	0.165	0.000	0.014	0.785
3	3.363	0.029	0.637	1.584	0.083	0.187	0.000	0.169	0.000	0.011	0.799
4	3.309	0.046	0.691	1.581	0.107	0.164	0.000	0.152	0.000	0.009	0.798
5	3.301	0.056	0.699	1.596	0.059	0.196	0.000	0.133	0.000	0.010	0.844
BB-2 (Bobai)											
1	3.295	0.009	0.705	1.657	0.104	0.134	0.002	0.135	0.000	0.014	0.829
2	3.292	0.020	0.708	1.747	0.009	0.121	0.001	0.160	0.000	0.016	0.782
3	3.324	0.013	0.676	1.682	0.033	0.200	0.000	0.112	0.000	0.014	0.840
4	3.267	0.020	0.733	1.617	0.152	0.097	0.000	0.156	0.000	0.015	0.828
5	3.308	0.010	0.692	1.592	0.175	0.075	0.002	0.200	0.000	0.018	0.780
HP-1 (Hepu)											
1	3.260	0.014	0.740	1.640	0.171	0.069	0.000	0.163	0.000	0.030	0.758
2	3.293	0.029	0.707	1.647	0.075	0.157	0.002	0.132	0.000	0.021	0.823
3	3.192	0.027	0.808	1.636	0.159	0.058	0.001	0.138	0.000	0.029	0.894
4	3.311	0.018	0.689	1.692	0.042	0.172	0.001	0.125	0.000	0.014	0.806
5	3.248	0.033	0.752	1.678	0.093	0.141	0.002	0.103	0.000	0.011	0.806
HT-1 (Hetai)											
1	3.225	0.000	0.775	1.811	0.038	0.081	0.000	0.116	0.004	0.016	0.812
2	3.255	0.004	0.745	1.831	0.000	0.091	0.001	0.106	0.000	0.012	0.830
3	3.309	0.009	0.691	1.800	0.000	0.102	0.000	0.091	0.000	0.016	0.853
4	3.204	0.008	0.796	1.865	0.000	0.080	0.001	0.079	0.000	0.021	0.825
5	3.177	0.009	0.823	1.813	0.068	0.032	0.000	0.125	0.000	0.015	0.816
HT44 (Hetai)											
1	3.203	0.018	0.797	1.758	0.091	0.030	0.002	0.155	0.000	0.023	0.783
2	3.131	0.011	0.869	1.829	0.092	0.004	0.001	0.110	0.000	0.035	0.799
3	3.087	0.035	0.913	1.901	0.017	0.039	0.000	0.056	0.000	0.052	0.780
4	3.114	0.024	0.886	1.767	0.129	0.000	0.000	0.126	0.000	0.034	0.813
5	3.127	0.026	0.873	1.712	0.160	0.000	0.000	0.162	0.000	0.027	0.802

See Fig. 2 for the sampling locations. The molecular components of muscovites were calculated based on electrovalence equilibrium criteria, assuming the number of O anion per formula unit (p.f.u.) being 11, where the separation of Fe^{2+} and Fe^{3+} was conducted according to Droop (1987).

quartz ribbons and bands of mafic minerals. Farther south, in Hetai, mylonites and migmatites contain an array of steeply dipping foliations that strike approximately N60°E to N80°E, clearly different from the typical regional strike of N45°E (Fig. 2). S–C fabrics in mylonites at Hetai indicates dextral shear (Figs. 3a,b).

3.2. Shuiwen–Xiangshui segment

Crossing the Xi River near Xiangshui (Fig. 2), mylonitic bands (Fig. 3d) exposed in Cambrian–Ordovician siliciclastic rocks strike ~N45°E, comparable to those in the northern segment. Farther

south, the trend of the shear zone changes to N60–80°E, crossing the northern edge of the Yunkai massif, where it tangentially cuts a SW-vergent arcuate thrust structure (Fig. 2) related to dextral slip along the shear zone (Xia and Xie, 1993).

This part of the shear zone cuts through a Caledonian biotite granite (zircon U–Pb age of 418 Ma; Wang et al., 1998) (Fig. 2), which to the north is intruded by an undeformed Jurassic granite (GBGMR, 1985). Mylonitic belts of various sizes occur within the Caledonian granite, forming regionally metamorphosed rocks (Fig. 2). The shear zone contains a mylonitic foliation that strikes parallel to its margins, generally consistent with the orientation of schistosity and gneissosity in the metamorphic country rocks (Fig. 2). The NE–SW-oriented blocks of schists within this part of the shear zone are sigmoidal in shape, indicating dextral motion (Ling et al., 1992).

3.3. Hepu–Beiliu segment

The Hepu–Beiliu segment trends ~N45°E over approximately 200 km on the western edge of the Yunkai massif from Beiliu (NW part of the massif) to Hepu (close to Beibu Bay) (Fig. 2). The extent of the continuation of the shear zone to the southwest (into Beibu Bay) remains unknown.

Along this segment of the shear zone, Paleozoic formations are strongly sheared to produce mylonitic belts of ~2–500 m in width. Close to the Yunkai massif, shearing deformation affected metamorphic rocks and pre-Mesozoic granites, producing mylonitic schists, gneisses, and mylonitized granites. Away from the Yunkai massif, toward the Qinzhou belt, Paleozoic strata record relatively weak ductile deformation but contain many brittle fractures. Rocks within these shear belts record varying degrees of mylonitization, occurring as proto-, S–C-, or ultra-mylonites. This segment of the shear zone is dominated by a moderately to steeply dipping penetrative mylonitic foliation with a gently plunging of sub-horizontal mineral stretching lineation. Although the foliation strike and lineation trend vary slightly along the shear zone (Fig. 2), the angle between S and C foliations, as well as the lineation plunge indicates dextral shear, as also indicated by fabrics in quartzo–feldspathic mylonites (Figs. 3c,e,f).

3.4. Summary

To conclude, the occurrence of a steeply dipping foliation and gently plunging lineation clearly demonstrates the strike-slip nature of the Hepu–Hetai shear zone. All kinematic indicators observed in the field and in thin sections (e.g., fractured quartz porphyroclasts, rolling structures of feldspar, domino structures of mica, the angle between S and C foliations, and the preferred orientation of recrystallized quartz grains (Figs. 3a,b,c,e)) indicate a dextral sense of shear over the entire shear zone.

Based on the experiential method of Otsuki (1978), assuming that total displacement along a shear zone is equal to 50 times its width, approximately 500 km of dextral slip is estimated for the Hepu–Hetai shear zone based on its average width of 10 km (range in width: 7.5–12.5 km). In addition, assuming the Dian–Qiong suture between the China–Vietnam border and central Hainan (see Section 2.3) was displaced by the shear zone, a minimum displacement of 500 km is estimated based on the extent of sporadically exposed basic rocks between Cenxi and central Hainan (Fig. 1B).

4. Temperature and pressure of ductile deformation along the Hepu–Hetai shear zone

4.1. Method

To constrain the temperature and pressure conditions of ductile deformation along the Hepu–Hetai shear zone, we undertook electronic probe microscopy (EPM) analyses of the geochemistry of juvenile minerals and analyses of synkinematic gas–liquid inclusions in quartz in samples of mylonite collected along the shear zone. Analyses were carried out at the State Key Laboratory for Mineral Deposits Research, Nanjing University, China, and sampling locations are shown in Fig. 2. EPM analyses of muscovite grains from five mylonitic samples were performed on a Jeol JXA-8100 operating at 15 kV accelerating potential, 20 nA beam current, and with a 20 s count time. The detection limit was 0.01 wt% for major elements. The reproducibility of measurements, based on analyses of SPI standards, was generally within 2% (2σ), and the analytical error was less than 5% (2σ) for elements occurring at concentrations of >5 wt% and less than 8% for those occurring at concentrations of <5 wt%. ZAF correction was applied to the analytical results. The homogenization temperatures of inclusions in quartz porphyroclasts were measured from four mylonitic samples using a Cmknm–Thms 600 instrument under a 30× objective lens. The obtained homogenization temperatures of inclusions and major element compositions of the muscovite grains are listed in Tables 1 and 2, respectively.

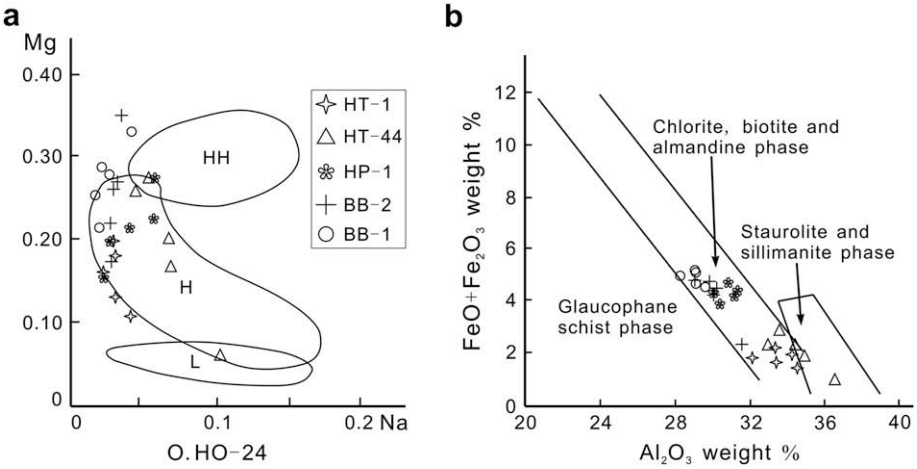

Fig. 4. Plots of the major elements of the synkinematic phengites in the mylonites from the Hepu–Hetai shear zone for the metamorphic condition. See Table 2 for the data used and Fig. 2 for the sampling locations. (a) Na–Mg plot, following Cipriani et al. (1971) and showing the metamorphic pressure, assuming O anion as 22 per formula unit, where *H* represents the pressure between 3 and 10 kbar. (b) Al_2O_3–FeO + Fe_2O_3 (wt %) plot, following Miyashiro (1972) and indicating the general metamorphic facies.

Table 3
$^{40}Ar/^{39}Ar$ analysis data of the juvenile muscovites in the mylonites from the Hepu–Hetai shear zone.

T	$^{39}Ar/^{36}Ar$	$^{40}Ar/^{36}Ar$	$^{37}Ar/^{39}Ar$	Age (Ma)	Error	$^{40}Ar^{*}\%$	$^{39}Ar\%$
Hetai 1; standard sample: age = 132.5 Ma, J = 1.07E-2							
2.00 W	275.67	2959.70	0.00	197.09	1.09	90.88	2.98
2.50 W	473.82	4956.28	0.00	192.28	0.85	94.32	5.73
3.00 W	387.78	4110.80	0.00	194.73	0.94	93.24	4.76
3.60 W	443.74	4703.44	0.00	194.71	0.90	94.04	6.52
4.10 W	222.80	2274.03	0.00	187.86	1.50	88.45	1.63
5.00 W	461.19	4841.15	0.00	192.93	0.94	94.20	5.30
5.90 W	370.66	3958.87	0.00	196.12	0.98	93.01	3.20
7.00 W	530.42	5731.87	0.00	198.31	0.85	95.05	9.97
8.00 W	537.04	5602.92	0.00	191.81	1.34	94.94	2.61
9.30 W	197.77	2071.84	0.00	192.56	2.12	87.47	1.70
12.00 W	503.04	5317.40	0.00	194.20	1.01	94.68	4.06
15.00 W	500.24	5207.22	0.00	191.40	0.82	94.58	5.76
18.00 W	530.35	5752.59	0.00	199.01	0.91	95.06	5.25
21.00 W	416.24	4436.26	0.00	195.73	0.89	93.71	5.11
25.00 W	573.81	6086.78	0.00	194.85	0.81	95.32	8.90
30.00 W	413.42	4426.79	0.00	196.59	0.84	93.69	8.63
35.00 W	444.81	4786.02	0.00	197.50	0.86	94.14	7.63
42.00 W	433.06	4622.43	0.00	196.01	0.98	93.94	6.11
Hetai 2; standard sample: age = 132.5 Ma, J = 1.07E-2							
2.00 W	277.03	2990.57	0.00	198.07	1.00	90.96	5.31
2.50 W	444.49	4584.00	0.00	189.67	0.93	93.89	5.52
3.00 W	462.06	4997.95	0.00	198.44	0.93	94.37	7.91
3.50 W	383.87	4065.75	0.00	194.53	1.04	93.18	4.43
4.00 W	520.36	5574.06	0.00	196.62	0.86	94.92	9.28
4.70 W	404.04	4362.91	0.00	198.12	0.90	93.61	6.04
6.00 W	476.35	5145.21	0.00	198.17	0.90	94.52	9.66
7.00 W	433.05	4694.53	0.00	198.86	0.89	94.03	8.13
8.00 W	320.68	3493.69	0.00	199.80	0.93	92.15	6.88
9.00 W	334.76	3640.16	0.00	199.44	0.96	92.44	4.40
11.00 W	258.19	2790.64	0.00	198.30	1.12	90.38	2.93
14.00 W	346.70	3764.40	0.00	199.16	1.08	92.67	5.35
19.00 W	424.03	4664.97	0.00	201.65	0.96	93.99	7.37
25.00 W	393.31	4348.91	0.00	202.62	0.90	93.59	8.28
32.00 W	345.50	3767.93	0.00	199.99	0.91	92.68	8.50
Datong 1; standard sample: age = 132 Ma, J = 1.22E-2							
440 °C	44.72	310.23	4.54	7.5	5.31	4.74	1.27
520 °C	69.17	335.68	3.74	13.21	2.24	11.95	1.82
600 °C	185.64	970.40	1.47	81.13	0.59	69.43	3.67
680 °C	299.73	2230.06	0.98	141.62	0.27	86.65	6.41
715 °C	361.35	3238.76	0.81	176.95	1.25	90.79	7.36
750 °C	244.61	2267.45	1.93	175.22	1.27	86.89	4.32
810 °C	679.37	7284.93	0.51	220.75	1.19	95.87	13.1
840 °C	626.14	6427.63	0.52	210.73	0.44	95.32	9.09
870 °C	667.64	6675.41	0.66	205.9	0.56	95.49	7.31
900 °C	716.83	7445.65	0.59	214.41	0.44	95.95	8.78
930 °C	484.02	4823.21	0.74	201.79	0.43	93.79	6.07
980 °C	621.52	6469.99	0.54	213.6	0.44	95.35	7.08
1030 °C	546.34	5689.50	0.52	212.35	0.40	94.73	6.63
1130 °C	678.46	7178.52	0.32	217.86	0.28	95.8	9.71
1340 °C	405.77	4211.28	0.47	207.82	0.36	92.91	7.4
Datong 2; standard sample: age = 132.5 Ma, J = 1.07E-2							
T (°C)	$^{39}Ar/^{36}Ar$	$^{40}Ar/^{36}Ar$	$^{37}Ar/^{39}Ar$	Age (Ma)	Error	$^{40}Ar^{*}\%$	$^{39}Ar\%$
2.00 W	465.39	4584.95	0.00	181.57	1.23	93.89	2.24
2.50 W	529.54	5551.32	0.00	192.61	0.98	94.89	2.58
3.00 W	693.67	7810.44	0.00	206.08	0.98	96.31	3.72
3.50 W	797.07	9194.47	0.00	210.85	0.88	96.84	4.46
4.00 W	877.42	10,220.18	0.00	212.79	0.91	97.14	5.74
4.70 W	804.56	9068.43	0.00	206.29	0.87	96.79	5.88
5.40 W	976.58	11,618.38	0.00	217.07	0.91	97.47	7.91
6.40 W	765.21	8596.31	0.00	205.64	0.93	96.63	5.00
7.00 W	743.17	8396.98	0.00	206.76	1.00	96.55	4.40
7.60 W	649.06	7031.50	0.00	198.70	0.93	95.92	2.85
9.00 W	766.59	8737.93	0.00	208.48	1.13	96.68	4.11
10.50 W	651.66	6991.26	0.00	196.87	1.07	95.89	3.27
12.20 W	859.44	10,125.22	0.00	215.08	0.90	97.12	5.40
14.00 W	924.71	10,848.64	0.00	214.23	1.02	97.30	4.60
16.20 W	634.66	7715.10	0.00	221.53	0.96	96.27	7.51
18.50 W	971.92	11,545.09	0.00	216.76	0.91	97.46	7.36
21.00 W	948.83	11,174.04	0.00	215.01	0.88	97.38	6.99
24.50 W	937.21	10,927.06	0.00	212.98	1.16	97.32	5.04
28.00 W	1062.80	12,630.02	0.00	216.85	0.98	97.67	4.63
36.00 W	1067.50	13,087.30	0.00	223.30	0.89	97.75	6.31

See Fig. 2 for the sampling sites. Note that samples were tested in two batch: first on Datong 1 with T by Celsius (°C) and second on the rest three with T by Power (W).

4.2. Results

We analyzed gas–liquid inclusions that occur along micro-fissures in quartz grains. These micro-fissures, which are similar in orientation to the mylonitic foliation and commonly extend across adjacent quartz grains, are considered to be syntectonic in origin. Regardless of any uncertainties in the estimated temperatures, each of the four analyzed samples records two sets of trapped temperatures (Table 1). This pattern is especially prominent for sample HT-44, which records temperatures of 469–496 °C and 303–312 °C, despite the limited amount of data. The higher trapped temperatures in HT-44 are in good agreement with the decrepitation temperatures of 440–510 °C reported by Liu et al. (2005) for samples from the same location as those analyzed in the present study. Samples BB-1 and BB-2 record a set of higher temperature in the range of 372–402 °C and a set of lower temperatures below 333 °C. Sample HP-1 records a narrower range of higher temperatures (404–446 °C) and a lower temperature of 333 °C.

Therefore, a thermal event with a moderate peak temperature (372–496 °C) was responsible for the ductile deformation recorded within the shear zone, possibly overprinted by a relatively low-temperature (298–333 °C) event. The estimated peak temperature is compatible with the micro-textures observed within mylonites (Figs. 3a–c), which indicate a deformation temperature of 350–500 °C based on the fact that quartz grains record ductile creep and feldspar porphyroclasts retain their pre-deformation shape (Tullis and Yun, 1977; Gapais, 1989).

The peak temperatures estimated for the four analyzed samples show a negative correlation with their respective average Si contents (p.f.u.) of juvenile phengite grains (Table 2). BB-1 has the highest average Si number (3.32), followed by BB-2 (3.30), HP-1 (3.26), and HT-44 (3.13). In contrast to the negative effect of increasing temperature on the Si number of phengite, the increasing pressure has a positive effect. Thus, in the present case it is possible to estimate the approximate stress of deformation based on the relationship between the Si content, temperature, and pressure (*Si–T–P*) of phengite (Velde, 1965; Massonne and Schreyer, 1987), assuming that the late-stage of low-temperatures (298–333 °C) made only a slight contribution to the Si content. As expected, samples BB-1 and BB-2 yield the highest pressures (7.7 and 7.2 kbar, respectively) based on their average trapped temperatures. HP-1 yields a medium pressure of 5.8 kbar, and HT-44 yields the lowest pressure of 4.2 kbar. Sample HT-1, for which inclusion data are unavailable, possibly shares the same trapped temperature as HT-44, given that the two samples were collected from the same site, although they record contrasting Si contents. The pressures estimated for sample HT-1 cluster around 6.5 kbar. Hence, over the entire shear zone, ductile deformation possibly occurred at an intermediate pressure (4.2–7.7 kbar) and temperature (372–496 °C). This finding is supported by the distribution of data on an Mg–Na plot for phengite, in which most of the samples plot in the field of 3–10 kbar (Fig. 4a). In an Al_2O_3–FeO_T plot, all the samples fall into the regime of the chlorite–biotite–almandine phase, which is indicative of greenschist facies metamorphism (Fig. 4b).

5. $^{40}Ar/^{39}Ar$ geochronology

5.1. Method

To establish the timing of ductile deformation, we undertook $^{40}Ar/^{39}Ar$ radiometric dating of synkinematic phengite grains from four samples of mylonite collected from the shear zone (Fig. 2). Standard mineral-separation techniques were employed, and analyses were performed using the incremental release technique. The samples chosen for $^{40}Ar/^{39}Ar$ analysis were first irradiated for ca. 90 hat the reactor housed in the Institute for Nuclear Physics and Chemistry, China Academy of Engineering Physics, Mianyang, using the Chinese Standard Sample ZBH2506 (biotite, 132.5 Ma; Wang et al., 2005) as a flux monitor. $^{40}Ar/^{39}Ar$ step-heating analyses of the samples were performed using a Micromass GV5400 Mass Spectrometer at the Argon Isotope Laboratory of the Guangzhou Institute of Geochemistry, Chinese Academy of Sciences, Guangzhou, following the technique described by Qiu (2006). The data and estimated analytical precision ($\pm\sigma$) were corrected for system blanks, mass discrimination, and interfering neutron reactions with Ca, Cl and K. The obtained $^{40}Ar/^{39}Ar$ ages were calculated using the ArArCALC software package (Koppers, 2002). The $^{40}Ar/^{39}Ar$ analytical data and resultant ages are presented in Table 3 and Fig. 5, respectively.

5.2. Results

Two phengite samples, Hetai 1 and Hetai 2, from Hetai in the northernmost segment of the shear zone (Fig. 2), show consistent age spectra (Fig. 5). Hetai 1, which produces a slightly less regular age spectrum, yields a 195 ± 1 Ma plateau age calculated based on nearly 100% of ^{39}Ar released; the corresponding isochronal age is 195.2 ± 4.7 Ma. The oldest single-step age obtained is 199 Ma; the youngest is 188 Ma. A slightly older plateau age of 198.9 ± 1.2 Ma is obtained for Hetai 2 based on nearly 100% of ^{39}Ar degassed. The corresponding isochronal age is 196.9 ± 5.6 Ma, and the oldest single-step age is 202 Ma.

Samples DT1 and DT2 were collected from Datong (Fig. 2). DT1 displays a composite age spectra (Fig. 5), with a plateau age of 213 ± 4 Ma calculated based on 75% of ^{39}Ar released. The oldest single-step age is as old as 221 Ma, obtained for a degassing temperature of 810 °C, which could represent the presence of excessive Ar. The lower-temperature steps show a clear overprinting pattern; two lower-temperature steps obtained at 12% released Ar yield an integrated age of 176 Ma. This Early Jurassic age is generally consistent with the ages obtained at Bobai (GBGMR, 1985; Peng et al., 1995) in the southern segment of the shear zone.

DT2 displays a relatively irregular age spectrum with a plateau age of 211.6 ± 3.4 Ma, and shows no prominent composite pattern. The first step of the lowest-temperature increment indicates an overprinting age of 181.6 Ma corresponding to a later tectonothermal event (as also observed in DT1). The oldest single-step age of 223 Ma is obtained in the last step of high-temperature increments with respect to the relatively retentive portion of radiogenic Ar in the mineral lattice; this age could represent the closure age of the Ar/Ar system.

5.3. Interpretation

As described in Section 4.2, the shear zone experienced ductile deformation at an intermediate temperature (372–496 °C); however, the Ar/Ar system in muscovite is generally believed to have a closure temperature of 390 ± 45 °C (Dodson, 1973; Hames and Bowring, 1994). Thus, it is likely that the Ar/Ar system within the analyzed muscovite grains was completely reset under the temperature conditions of deformation in the shear zone, meaning that the ages obtained in the present study may reflect the cooling history following the final thermotectonic event. The plateau ages obtained for samples from Datong and Hetai differ by up to 18 Ma, possibly reflecting the progressive northward migration of shear deformation or exhumation.

A 240–250 Ma tectonic event is recognized across Indochina (Lepvrier et al., 2004), and continuous magmatism throughout the period of 269–201 Ma has been identified along the Hepu–Hetai shear zone and adjacent areas. These observations, combined with

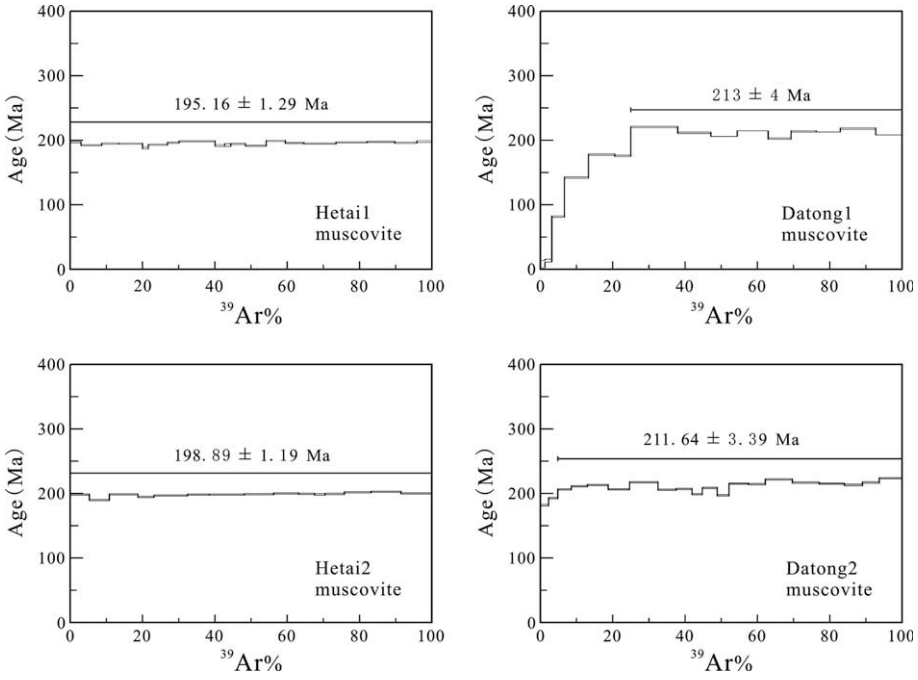

Fig. 5. $^{40}Ar/^{39}Ar$ age spectra of the synkinematic muscovites from the mylonites along the Hepu–Hetai shear zone. See Table 3 for the data employed and Fig. 2 for the sampling locations.

the age data obtained in the present study, indicate that this tectonic event, which began in the Early Triassic or Late Permian, could have persisted into the Late Triassic but not beyond the Early Jurassic, as constrained by the ages of 195–198 Ma obtained at Hetai. In addition, the low-temperature degassed age (176–181 Ma) obtained for the Datong samples may represent a Middle Jurassic thermal event that partially reset the Ar/Ar system of muscovite, coincident with the 177–178 Ma age of metamorphic rocks near Bobai (GBGMR, 1985; Peng et al., 1995).

6. Tectonic model

6.1. Irregular continental margin of southern China

Lithofacies and paleogeographic data (Fig. 6) indicate the occurrence of a Late Paleozoic bay on the passive southern margin of South China, bounded to the east by the Yunkai Promontory and to the west by the Kangdian massif. Both of these massifs with Precambrian basement contained emergent land and were largely

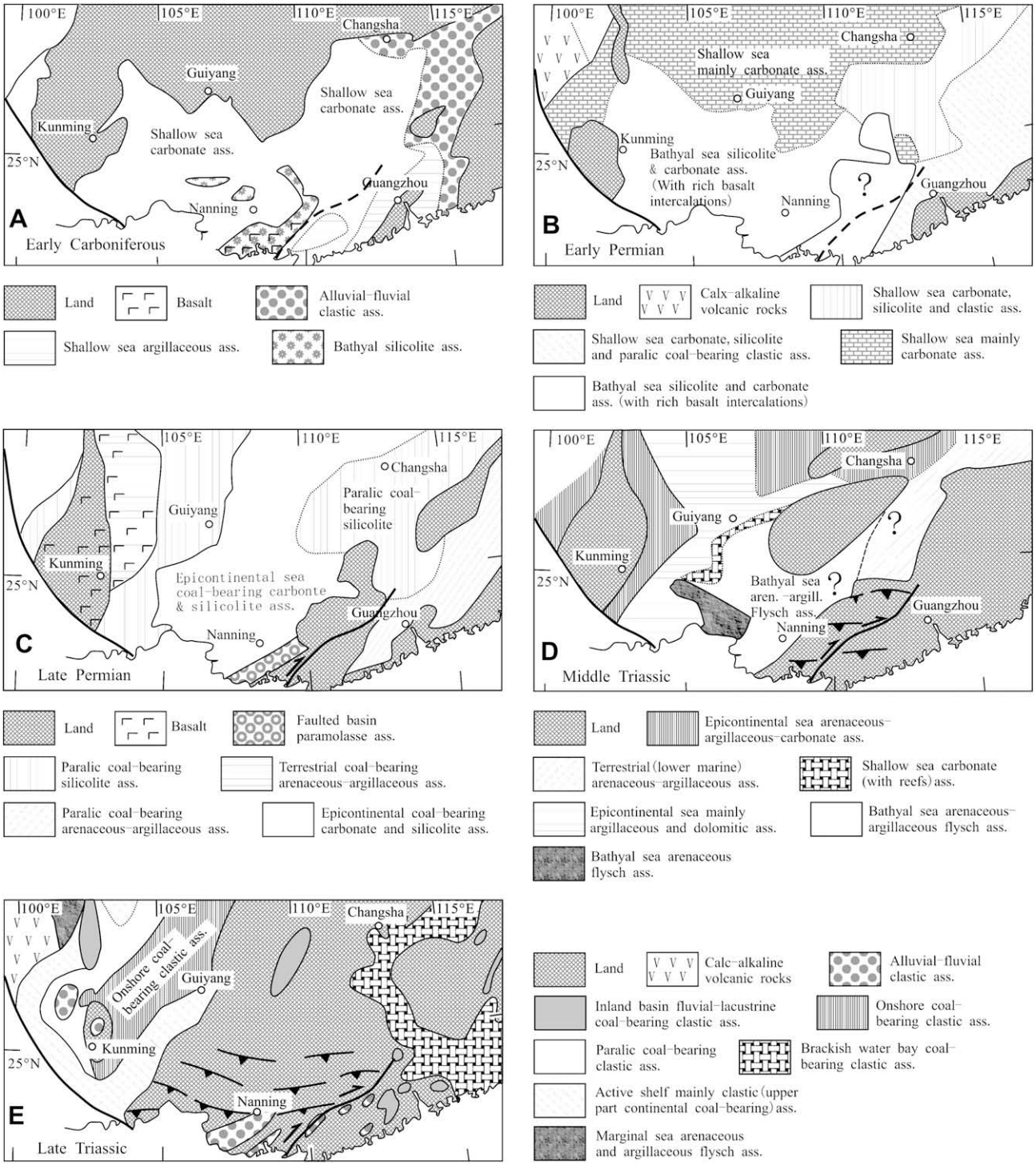

Fig. 6. Carboniferous–Triassic paleogeography of the southern margin of South China, indicative of an irregular passive continental margin of South China during the Late Paleozoic to Middle Triassic. Also shown is the location of the Hepu–Hetai shear zone. Revised after Zhao and Ding (1996) and Lehrmann et al. (2007).

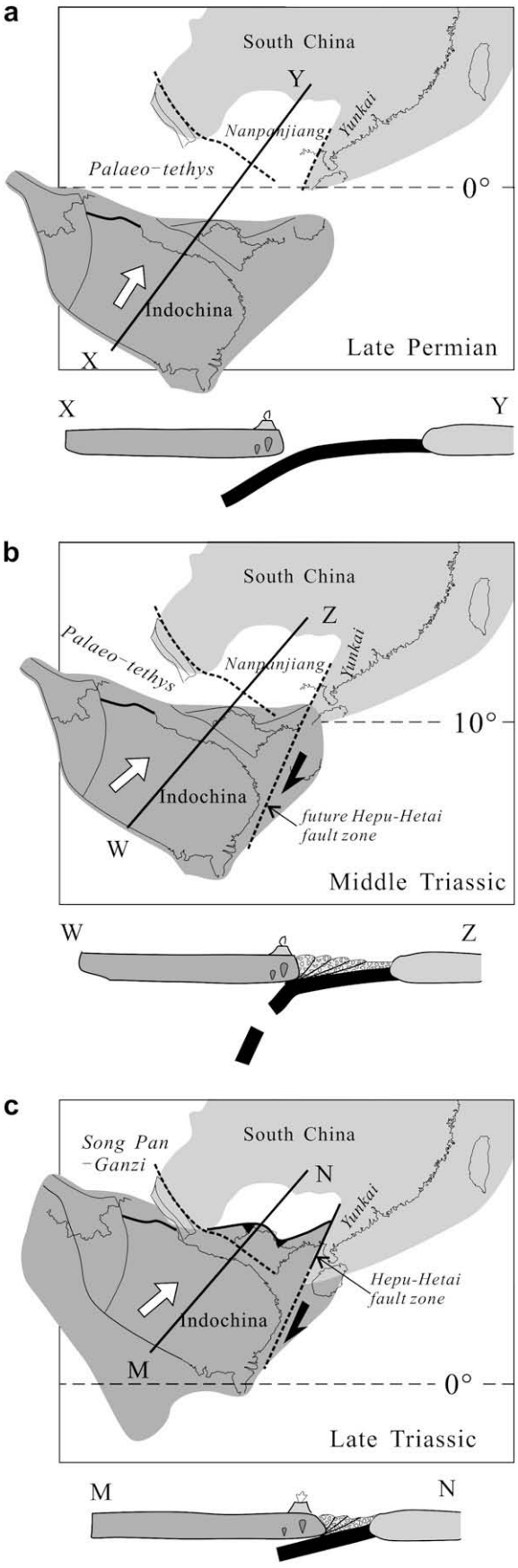

Fig. 7. Tectonic evolution of eastern Asia during the latest Paleozoic to Early Mesozoic.

surrounded by a shallow carbonate platform during the Late Paleozoic (Zhang, 1997). Within the bay, however, a deep-water starved basin developed, along with several isolated carbonate platforms. This pattern of sedimentation continued until the end of the Early Triassic. The bay was infilled by turbidite deposits during the Middle Triassic (Lehrmann et al., 2007), and the entire area was uplifted during the Late Triassic. Thus, the setting of two resistant promontories and an intervening marine basin indicates an irregular geometry for the passive southern continental margin of South China from the Late Paleozoic to Early Triassic.

6.2. Hepu–Hetai dextral shear zone: product of the penetration of the Yunkai Promontory of South China into Indochina

It can be concluded that the Hepu–Hetai shear zone had a history of dextral ductile strike-slip from the Late Permian, ceasing by the earliest Early Jurassic. Previous workers have proposed that during this period the shear zone acted as either a thrust fault or detachment fault (Zhang and Yu, 1992; Wang et al., 1994; Peng et al., 1995); however, this view is inconsistent with existing kinematic data, the steep dip of the mylonitic foliation, the sub-horizontal orientation of the stretching lineation, and indicators of dextral shear sense.

The mafic rocks indicative of suturing in the interior of the southern Chinese mainland could have resulted from dextral displacement along the shear zone, assuming these rocks were originally aligned with those in central Hainan. This dextral displacement along the shear zone possibly resulted from collision between South China and Indochina along the Dian–Qiong suture during the latest Permian to Triassic. According to this scenario, the collage between Indochina and South China developed in response to penetration of the rigid Yunkai Promontory into Indochina. Consequently, the relatively weak Indochina block was torn apart along the western edge of the Yunkai Promontory, thereby initiating the dextral Hepu–Hetai shear zone.

This strong penetration of the Yunkai Promontory into Indochina was possibly initiated during the latest Permian (Fig. 7A), based on the age of voluminous molasse deposits in central Hainan and the eastern part of the Nanpanjiang Basin (GBGMR, 1988). The extensive Middle Triassic siliciclastic turbidites found in the basin represent the peak of the collision (Fig. 7B). The collision possibly led to the early termination of deposition upon the southernmost platform in the Nanpanjiang Basin and the development of a volcanic arc at the southern margin of South China, as proposed by Lehrmann et al. (2007). By the end of the Carnian (216 Ma), the accretion of Indochina to South China was essentially complete (Fig. 7C) based on the 212–213 Ma Ar/Ar age obtained for mylonitic rocks form Datong and the development of a regional Norian unconformity across SE Asia. Inland compression that generated dextral displacement along the shear zone possibly continued until the Late Triassic, but not beyond the earliest Early Jurassic, as suggested by a 195–198 Ma cooling age obtained at Hetai. Subsequently, this region was affected by deformation associated with subduction of the West Pacific Plate based on the 176–181 Ma overlapping age obtained for DT1. The accretion of Indochina to mainland Asia also possibly contributed to the final suturing of South and North China (Zhang, 1997; Zhang et al., 2007).

7. Conclusions

The NE–SW-trending Hepu–Hetai shear zone, which is characterized by right-lateral ductile deformation of up to 500 km, is possibly a product of the Indosinian Orogeny. The shear zone was initiated during the Late Permian when the Yunkai Promontory penetrated into Indochina. Following the final suturing of Indochina

and South China during the Late Triassic (212–213 Ma), dextral displacement upon the shear zone continued until the earliest Jurassic (195–198 Ma). Shear deformation within the shear zone occurred under intermediate pressure-temperature conditions of the greenschist facies (372–496 °C, 4.2–7.7 kbar).

Acknowledgements

This study was supported by the Hundred Talents Project of Chinese Academy of Science. We are grateful to X.M. Chen and H.N. Qiu for analytical support, to X.C. Tang and J.C. Wang for fieldwork assistance, and to M. Egydio-Silva and D.J. Lehrmann for constructive and thoughtful review comments, which greatly improved the manuscript. This is contribution No. IS-1064 from GIGCAS.

References

CAGS (Chinese Academy of Geological Science), 1975. Asian Geology Map (1:5 000 000). Geological Publishing House, Beijing.
Cipriani, C., Sassi, F.P., Scolari, A., 1971. Metamorphic white micas definition of paragenetic fields. Schweizerische Mineralogische und Petrographische Mitteilungen 51, 259–302.
Dodson, M.H., 1973. Closure temperature in cooling geochronological and petrological systems. Contributions to Mineralogy and Petrology 40, 259–274.
Droop, G.T.R., 1987. A General equation for estimating Fe^{3+} concentrations in the ferromagnesian silicates and oxides from microprobe analyses, using stoichiometric criteria. Mineralogical Magazine 51, 431–435.
Enos, P., Jiayong, W., Lehrmann, D.J., 1998. Death in Guizhou – Late Triassic drowning of the Yangtze carbonate platform. Sedimentary Geology 118, 55–76.
Findlay, R.H., Phan, T.T., 1997. The structural setting of the Song Ma region, Vietnam and the Indochina plate boundary problem. Gondwana Research 1, 11–33.
Gapais, D., 1989. Shear structures within deformed granites: mechanical and thermal indicators. Geology 17, 1144–1147.
GBGMR (Guangdong Bureau of Geology and Mineral Resources), 1988. Regional Geology of Guangdong Province. Geological Publishing House, Beijing.
GBGMR (Guangxi Bureau of Geology and Mineral Resources), 1985. Regional Geology of Guangxi Zhuang Autonomous Region. Geological Publishing House, Beijing.
Hames, W.E., Bowring, S.A., 1994. An empirical evaluation of the argon diffusion geometry in muscovite. Earth and Planetary Science Letters 124, 161–167.
Hsü, K.J., Li, J.L., Chen, H.H., Wang, Q.C., Sun, S., Sengör, A.M.C., 1990. Tectonics of South China: key to understanding west Pacific geology. Tectonophysics 183, 9–39.
Huang, G.C., Wang, X.W., Yang, S.Y., Chen, L.Q., Ling, J.S., 2001. Chronological evidence for the existence of the Meso- to Paleo-Proterozoic basement in the Yunkai uplift area. Regional Geology of China 20, 194–199.
Hutchison, C.S., 1993. Gondwana and Cathysian blocks, Paleotethys sutures and Cenozoic tectonics in south-east Asia. Geologische Rundschau 82, 388–405.
Koppers, A.A.P., 2002. ArArCALC-software for $^{40}Ar/^{39}Ar$ age calculations. Computer Geosciences 28, 605–619.
Lacassin, R., Leloup, P.H., Phan, T.T., Tapponnier, P., 1998. Unconformity of red sandstones in N. Vietnam: field evidence for Indosinian Orogeny in Northern Indochina? Terra Nova 10, 106–111.
Lehrmann, D.J., Pei, D.H., Enos, P., Minzoni, M., Ellwood, B.B., Orchard, M.J., Zhang, J.Y., Wei, J.W., Dillett, P., Koenig, J., Steffen, K., Druke, D., Druke, J., Kessel, B., Newkirk, T., 2007. Impact of differential tectonic subsidence on isolated carbonate-platform evolution: Triassic of the Nanpanjiang Basin, south China. American Association of Petroleum Geologists Bulletin 91, 287–320.
Lepvrier, C., Maluski, H., Vu, V.T., Leyreloup, A., Phan, T.T., Nguyen, V.V., 2004. The Early Triassic Indosinian Orogeny in Vietnam (Truong Son Belt and Kontum Massif): implications for the geodynamic evolution of Indochina. Tectonophysics 393, 87–118.
Li, X.H., Zhou, H.W., Ding, S.J., Lee, C.Y., Zhang, R.J., Zhang, Y.M., Ge, W.C., 2000a. Metamorphosed mafic rocks with N-type MORB geochemical features in Hainan Islands: remnants of the Paleo–Tethys oceanic crust? Chinese Science Bulletin 45, 956–960.
Li, X.H., Zhou, H.W., Ding, S.J., Lee, C.Y., Zhang, R.J., Zhang, Y.M., Ge, W.C., 2000b. Sm–Nd isotopic constraints on the age of the Bangxi–Chenxing ophiolite in Hainan Island: implications for the tectonic evolution of eastern Paleotethys. Acta Petrologica Sinica 16, 425–432.
Li, X.H., Zhou, H.W., Chung, S.L., Ding, S.J., Liu, Y., Lee, C.Y., Ge, W.C., Zhang, Y., Zhang, R., 2002. Geochemical and Sm–Nd isotopic characteristics of metabasites from central Hainan Island, South China and their tectonic significance. Island Arc 11, 193–205.
Liang, X.Q., Li, X.H., 2005. Late Permian to Middle Triassic sedimentary records in Shiwandashan Basin: implication for the Indosinian Yunkai Orogenic Belt, South China. Sedimentary Geology 177, 297–320.
Ling, J.S., Qiu, Y.S., Cen, C.T., Li, W.Z., Kang, D.C., 1992. A Study of Metallogenic Conditions of Gold Prospective Regions in Yunkai Mountains and Neighbouring Areas. Geological Publishing House, Beijing.
Liu, W., Huang, M.X., Quyang, Y.F., 2005. Characteristics of mineralization fluids in the Hetai gold deposit of Guangdong. Mineral Resources and geology 19 369–474.
Massonne, H.J., Schreyer, W., 1987. Phengite geobarometry based on the limiting assemblage with K-feldspar, phlogopite, and quartz. Contributions to Mineralogy and Petrology 96, 212–224.
Mercier, R.J., 1977. Stress in the lithosphere: inferences from steady-state flow of rocks. Pure and Applied Geophysics 115, 199–226.
Metcalfe, I., 2002. Permian tectonic framework and paleogeography of SE Asia. Journal of Asian Earth Science 20, 551–566.
Miyashiro, A., 1972. Metamorphism and Metamorphic Belts. John Wiley & Sons, New York.
Otsuki, K., 1978. On the relationship between the width of a shear zone and the displacement along fault. Journal of the Geological Society of Japan 84, 661–669.
Peng, S.M., Duan, J.R., He, S.X., Wu, G.Y., Zhang, F.S., Chen, S.X., 1990. The Xinzhou fold-thrust nappe in north Guangdong. Guangdong Geology 5, 79–91.
Peng, S.M., Fu, L.F., Zhou, G.Q., 1995. Tectonic Evolution of Yunkai Massif and its Shearing Anatectic Origin of Gneissic Granitic Rocks. China University of Geosciences Press, Wuhan, pp. 43-85.
Peng, S.B., Jin, Z.M., Fu, J.M., He, L.Q., Cai, M.H., Liu, Y.H., 2006a. The geochemical evidences and tectonic significance of Neoproterozoic ophiolite in Yunkai area, western Guangdong Province, China. Acta Geologica Sinica 80, 814–825.
Peng, S.B., Jin, Z.M., Liu, Y.H., Fu, J.M., He, L.Q., Cai, M.H., Wang, Y.B., 2006b. Petrochemistry, chronology and tectonic setting of strong peraluminous anatectic granitoids in Yunkai Orogenic Belt, western Guangdong Province. Earth Science-Journal of China University of Geosciences 31, China. 110-120.
Potter, R.W., 1977. Pressure corrections got f1uid-inclusions on homogenization temperatures based on the volumetric properties of the system NaCI–H2O. Journal of Research. US Geological Survey 5, 603–607.
Qin, X.F., Zhou, F.S., Hu, G.A., Li, G.N., Xie, L.F., Zhou, K.H., Huang, X.Q., Pan, Y.W., 2005. First discovery of MORB volcanic rock and its tectonic significance on the north margin of the Yunkai block, southeastern Guangxi. Geological Science and Technology Information 24, 20–24.
Qin, X.F., Pan, Y.M., Li, J., Li, R.S., Zhou, F.S., Hu, G.A., Zhong, F.Y., 2006. Zircon SHRIMP U–Pb geochronology of the Yunkai metamorphic complex in southeastern Guangxi, China. Geological Bulletin of China 25, 553–559.
Qiu, H.N., 2006. Construction and development of new Ar–Ar laboratories in China: insights from GV-5400 Ar–Ar laboratory in Guangzhou Institute of Geochemistry, Chinese Academy of Sciences. Geochimica 35, 133–140.
Tullis, J., Yun, R.H., 1977. Experimental deformation of dry Westerly Granites. Journal of Geophysical Research 82, 5705–5718.
Twiss, R.J., 1977. Theory and applicability of a recrystallized grain size paleopiezometer. Pure and Applied Geophysics 5, 337–340.
Velde, B., 1965. Phengite micas: synthesis, stability, and national occurrence. American Journal of Science 263, 886–913.
Wang, J.C., Wang, Z.Y., Geng, W.H., Yin, Y.Q., Yang, M.S., 1994. The discovery and significance of the large-scale detachment faults in the wedge of the Yunkai massif. Chinese Science Bulletin 39, 1886–1888.
Wang, J.H., Sun, D.Z., Chang, X.Y., Deng, S.X., Zhang, H., Zhou, H.W., 1998. U–Pb dating of the Napeng granite at the NW margin of the Yunkai block, Guangdong, South China. Acta Mineralogica Sinica 18, 130–133.
Wang, J.H., Tu, X.L., Sun, D.Z., 1999. U–Pb dating of anatectic migmatites at Gaozhou in the Yunkai block, western Guangdong, China. Geochimica 28, 231–238.
Wang, F., He, H.Y., Zhu, R.X., Sang, H.Q., Wang, Y.L., Yang, L.K., 2005. Intercalibration of international and domestic $^{40}Ar/^{39}Ar$ dating standards. Science in China. Series D 35, 461–470.
Wang, Y.J., Fan, W.M., Gawood, P.A., Ji, S.C., Peng, T.P., Chen, X.Y., 2007. Indosinian high-strain deformation for the Yunkaidashan tectonic belt, south China: kinematics and $^{40}Ar/^{39}Ar$ geochronological constraints. Tectonics 26, 1–21.
Wu, G.Y., Zhong, D.L., Zhang, Q., Ji, J.Q., 1999. Babu-Phu Ngu ophiolites: a geological record of Paleotethyan ocean bordering China and Vietnam. Gondwana Research 2, 554–557.
Wu, G.Y., Wu, H.R., Zhong, D.L., Kuang, G.D., Ji, J.Q., 2000. Volcanic rocks of Paleotethyan oceanic island and island-arc bordering Yunnan and Guangxi, China. Geoscience 14, 393–400.
Wu, G.Y., Ma, L., Zhong, D.L., Wu, H.R., Ji, J.Q., Kuang, G.D., Xu, K.D., 2001. Indosinian Turkic-type orogen bordering Yunnan and Guangxi: with reference to coupled basin evolution. Petroleum Geology and Experiment 23, 8–18.
Wu, G.Y., Ji, J.Q., He, S.D., Zhong, D.L., 2002. Early Permian magmatic arc in Pingxiang, Guangxi and its tectonic implications. Journal of Mineralogy and Petrology 22, 61–65.
Xia, L.H., Xie, S.X., 1993. Guizi arc structure in Luoding area and its tectonic mechanism. In: Qiu, Y.X., Chen, H.J. (Eds.), Geology and Tectonic Symposia of the Yunkaidashan and Neighboring Areas. Geological Publishing House, Beijing, pp. 60–65.
Ye, B.D., 1989. Isotopic age data from Yunkai area of Guangdong and Guangxi Provinces and their geologic implications. Guangdong Geology 4 (3), 39–55.
YNGMR (Yunnan Bureau of Geology and Mineral Resources), 1990. Regional Geology of Yunnan Province. Geological Publishing House, Beijing, pp. 45-201.
Zhang, K.J., 1997. North and South China collision along the eastern and southern North China margins. Tectonophysics 270, 145–156.
Zhang, B.Y., Yu, H.N., 1992. The genetic relationship of mylonites, migmatites and granites with special reference to the deep-level nappe structure in western Guangdong. Geological Review 38, 407–413.
Zhang, B.Y., Shi, M.Q., Yang, S.F., Chen, H.L., 1995. New evidence of the Paleotethyan orogenic belt on the Guangdong–Guangxi region, South China. Geological Review 41, 1–6.

Zhang, Z.L., Yuan, H.H., Nan, Y., 1998. Whole-grain zircon evaporation for age of Luoyu formation, Yunkai group. Journal of Mineral and Petrology 18 (11), 85–90.

Zhang, K.J., Xia, B.D., Liang, X.W., 2002. Mesozoic–Paleogene sedimentary facies and paleogeography of Tibet, western China: tectonic implications. Geological Journal 37, 217–246.

Zhang, B.Y., Zhang, H.X., Zhao, Z.H., Yang, S.F., Chen, H.L., Shi, M.Q., 2003. Permian island-arc basalt in west Guangdong and east Guangxi tectonic belt, South China: implications for the Paleotethys. Journal of Nanjing University (Natural Sciences) 39, 46–54.

Zhang, K.J., Cai, J.X., Zhu, J.X., Huang, Z.J., Shen, X.Z., 2007. Early Mesozoic overthrust tectonics around the Tanlu fault zone, eastern China: implications for the North and South China collision. Journal of the Geological Society of India 70, 584–594.

Zhao, Z.Q., Ding, Q.X., 1996. Regional Stratigraphy in Central and South Part of China. China University of Geosciences Press, Wuhan.

Zhong, D.L., Wu, G.Y., Ji, J.Q., Zhang, Q., Ding, L., 1998. Discovery of the ophiolites in southeastern Yunnan, China. Chinese Science Bulletin 43, 1364–1369.

Zhou, X.M., Sun, T., Shen, W., Shu, L., Niu, Y., 2006. Petrogenesis of Mesozoic granitoids and volcanic rocks in South China: a response to tectonic evolution. Episodes 29, 26–33.